Annual variation of coastal uplift in Greenland as an indicator of variable and accelerating ice mass loss

Qian Yang and Timothy H. Dixon

University of South Florida, Department of Geology, 4202 E Fowler Ave, Tampa, FL, 33620, USA (qianyang@mail.usf.edu)

Shimon Wdowinski

Marine Geology and Geophysics, Rosenstiel School of Marine and Atmospheric Science, University of Miami, Miami, FL, USA

[1] Seasonal melting of the coastal part of the Greenland ice sheet is investigated using GPS vertical displacement data from coastal stations, combined with data on atmospheric and ocean temperatures. Using a high pass filter and cubic spline models, we estimate five variables describing seasonal uplift, a proxy for proximal mass loss, including duration of the melt season and the amount of summer uplift. Our analysis shows both temporal and spatial variations of uplift. Southern coastal Greenland experienced anomalously large uplift in summer 2010, implying significant melting that year. However, the northwest coast did not experience significant change in uplift at that time. Our data suggest that a combination of warm summer air temperature and warm sub-surface ocean water temperature drove the large mass losses in 2010. Using the uplift pattern of 2008–2010, and comparing to atmospheric data and ocean water temperature data, we show that warm Irminger Water (IW) exerted significant influence on coastal melting in southeastern, southern and southwestern Greenland, reaching about 69°N in 2010. North of this, IW did not exert significant influence, in effect defining the northward limit of the sub-polar gyre for that year. Thus, short-term variability in the coastal GPS uplift signal can be used to infer an oceanographic parameter that has a critical influence on Greenland ice sheet health.

1. Introduction

[2] Significant mass loss of the Greenland ice sheet has been revealed in the last decade by the GRACE gravity mission [*Velicogna and Wahr*, 2006; *Velicogna*, 2009; *Chen et al.*, 2006; *Luthcke et al.*, 2006; *van den Broeke et al.*, 2009; *Jacob et al.*, 2012], satellite altimetry [*Krabill et al.*, 2004; *Zwally et al.*, 2005; *Thomas et al.*, 2006], mass accumulation/loss estimates [*Hanna et al.*, 2005; *Rignot and Kanagaratnam*, 2006; *Rignot et al.*, 2008], and GPS observations of coastal uplift [*Jiang et al.*, 2010; *Khan et al.*, 2010; *Bevis et al.*, 2012]. Recent studies detect considerable spatial and temporal variability of ice sheet mass change: prior to the 2010 melt season, mass loss appeared to be accelerating along the northwest coast, but slowing down in southeast Greenland since 2007 [*Khan et al.*, 2010; *Murray et al.*, 2010; *Chen et al.*, 2011]. Subsequently, *Box et al.* [2010] reported anomalously high air temperatures and melting in summer 2010 for much of coastal Greenland.

[3] Coastal uplift is a useful proxy for coastal mass loss and perhaps overall Greenland ice mass balance. Previous studies have demonstrated that accumulation and loss in the interior of Greenland are in approximate balance, while recent net losses are focused in marginal coastal areas [e.g., *Zwally et al.*, 2005; *Thomas et al.*, 2006; *Luthcke et al.*, 2006; *Rignot and Kanagaratnam*, 2006; *Wouters et al.*, 2008]. These coastal losses result in significant coastal uplift, reflecting the short-term, elastic response of the crust to mass unloading, and are readily measured by high precision GPS [*Jiang et al.*, 2010; *Khan et al.*, 2010; *Bevis et al.*, 2012]. Our previous study focused on decadal scale trends and demonstrated that decadal time series of the vertical position component were surprisingly well fit by a simple model of constant acceleration, with values for some Greenland stations, up to the end of the 2008 melt season, approaching $1 \, \text{mm/yr}^2$ [*Jiang et al.*, 2010]. More recent measurements suggest that this trend of accelerating melting and uplift is continuing, at least at some locations, with the 2010 melt season recording the largest uplift since measurements began at many localities [*Bevis et al.*, 2012].

[4] *Jiang et al.* [2010] also suggested that there was useful information in the annual variation of coastal uplift. In Greenland, ice mass change is regulated by two climate factors, atmospheric forcing [*Zwally et al.*, 2002; *Hall et al.*, 2008] and oceanic forcing [*van de Wal et al.*, 2008; *Holland et al.*, 2008; *Hanna et al.*, 2009; *Straneo et al.*, 2010, 2012;

Seale et al., 2011]. Atmospheric forcing can affect surface mass balance (SMB) by changing either or both the snow accumulation rate and the ablation rate. Also, melt water can influence the basal sliding rate. Oceanic forcing can increase submarine melting of marine-terminating outlet glaciers, resulting in rapid changes in calving rate, and inducing dynamic changes upstream, including glacier acceleration and thinning. For both atmospheric and oceanic forcing, most melting occurs during the warm summer months and at low elevations near the coast. Nevertheless, it may be possible to use the summer uplift signal to separate the various effects and elucidate controls on mass loss. In this paper, we focus on seasonal uplift patterns in GPS data by using a high pass filter and cubic spline fit to the vertical position time series. We investigate regional and temporal changes in annual uplift and, by implication, coastal melting, and attempt to separate the relative roles of oceanic versus atmospheric forcing.

2. Methods

2.1. GPS Data and Processing

[5] We analyzed all publicly available GPS data up to May 2011. Data from 18 continuous or semicontinuous GPS sites in the coastal region of Greenland are now available with at least 3 years of data, through the establishment of a remarkable network of reliable, high precision instruments [*Bevis et al.*, 2012] (Figure 1). We use the GIPSY-OASIS 5.0 software [*Zumberge et al.*, 1997] to process these data. Orbit parameters and clock products are provided by Jet Propulsion Laboratory (ftp://sideshow.jpl.nasa.gov/). We use the Global Mapping Function [*Boehm et al.*, 2006] to relate the atmospheric wet delay to elevation angle. An ocean tidal loading correction is applied to all sites by using model FES2004 [*Letellier*, 2004]. We first generate daily precise point position solutions for each station. We then adopt the Ambizap algorithm [*Blewitt*, 2008] to solve integer ambiguities for each station. The final ambiguity-fixed daily solutions are then aligned to the IGS05 reference frame [*Altamimi et al.*, 2007]. Errors associated with GPS reference frame instability are probably negligible for the short-term (2008–2010) comparisons that are the main focus of our study, although they could affect longer-term (decadal) time series.

[6] To isolate the effect of ice load variation from seasonal atmospheric loading, we apply an air
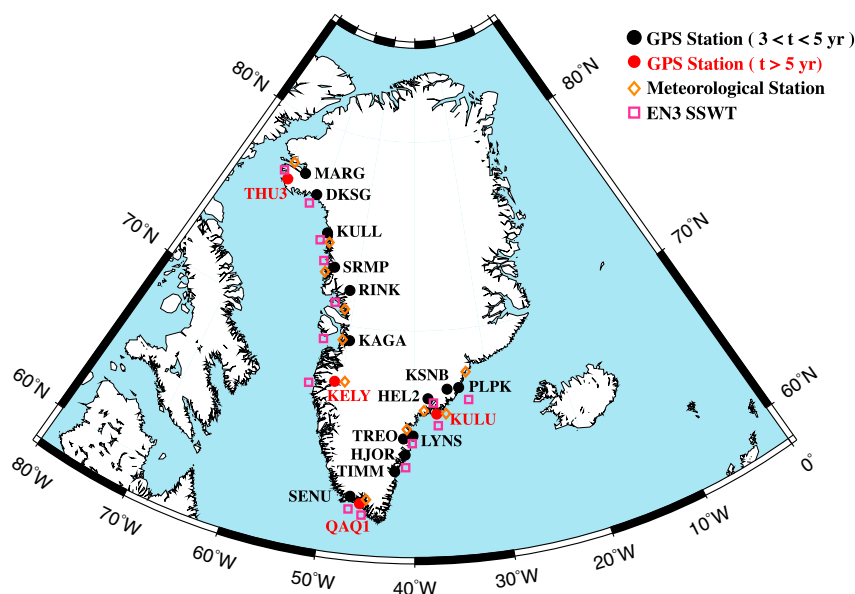
Figure 1. Map of Greenland showing location of GPS sites, meteorological stations, and other data used in this study. Red circles indicate GPS sites with more than 5 years of data. Black circles indicate sites with 3 to 5 years of data. Orange diamonds indicate meteorological stations. Pink squares indicate pixels of sub-surface water temperature produced by EN3 model.

pressure loading correction. We subtract precomputed Atmospheric Loading Displacements (http://gemini.gsfc.nasa.gov/aplo/) [*Petrov and Boy*, 2004] from the GPS vertical displacement time series. Details of this procedure are described in the supporting information section.

[7] We also considered the possibility of local snow loading as a source of annual uplift variability. Calculations suggest that the deformation caused by local snow load is less than 1 mm at most of our study sites (supporting information),[1] so we have ignored this effect.

2.2. Seasonal Uplift Analysis

[8] *Jiang et al.* [2010] assumed constant amplitude of annual uplift each year, a common assumption in GPS time series analysis. However, the data show significant annual variation, and it is this variation that we seek to quantify. Variable amplitude in the seasonal signal has been addressed in several ways [*Murray and Segall*, 2005; *Davis et al.*, 2006; *Bennett*, 2008; *Davis et al.*, 2012]. In this paper, we first use a high pass filter to isolate the seasonal signal by removing the secular component from the GPS time series. We then fit the residual GPS time series with a smoothing cubic spline. Based on the

spline model estimate (red solid line in Figure 2), we derive five variables that relate to mass loss: the timing (start and end time) and duration of summer melt season, the total amount of seasonal uplift (which relates to the total mass loss, including surface and sub-surface melting, runoff, calving, and dynamic thinning) for the local basin, and the rate of summer uplift (Figure 2). We chose a cubic
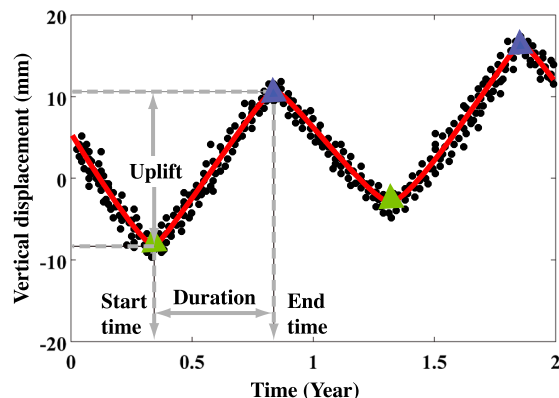
Figure 2. Hypothetical 2 year time series showing four parameters (start time, end time, duration, and uplift) defined for a melt season. Each black dot represents daily vertical position estimate. Red curve is best fit model. Blue triangles mark the maximum position value per year, and green triangles are the minimum value per year. A fifth parameter (rate of summer uplift) is the average slope of the curve between the start time and end time of uplift.

---

[1]All supporting information may be found in the online version of this article.

spline model because it is straightforward to apply and can identify the minima and maxima for each year without any assumptions concerning specific periodicity, which may vary from year to year.

[9] A key parameter in the cubic spline model is the smoothing, S. As the value of S increases, misfit decreases, but the "roughness" (complexity) of the model increases; at some point, more than one maxima and minima per year can result, which is generally unrealistic. Thus, there is a trade-off between goodness of fit and smoothing. A sensitivity study using various values of S allows us to define an optimum value by requiring a single crest and a single trough per year. The optimum smoothing parameter differs somewhat for each site because of variations in data quality and length of time series. We chose a compromise value ($S = 0.91$) and applied it to all sites to ensure that relative variations in estimated parameters can be compared across all the time series and regions in a consistent way. This value generates single minima and single maxima per year for 16 out of 18 sites. For sites THU3 and QAQ1, the analysis yields double peaks in 2007 and 2008, respectively, although one is smaller than the other. For these two sites, we remove the smaller crest and trough, using the larger one to estimate the five parameters of interest. These sites are marked with an asterisk in Table 1. Note that the seasonal uplift estimated in this way is somewhat conservative, especially for years with significantly different uplift compared to earlier years. This reflects the fact that our technique tends to damps extreme excursions, with the effect increasing as the degree of smoothing increases. All time series and their spline model fits are shown in the supporting information.

[10] Uncertainties for the parameter estimates are determined with a Monte Carlo approach. We report the mean value of a large number of estimates as the best estimate, with uncertainty defined at the one-sigma confidence level based on the bounds containing 68% of the estimated values. Details of this procedure are described in the supporting information section.

2.3. Surface Air Temperature Data and Analysis

[11] We obtained daily surface air temperature data from 11 meteorological stations in coastal Greenland provided by the Danish Meteorological Institute [*Carstensen and Jørgensen*, 2011]. All the stations are synoptic and observe surface air temperature and other weather parameters at 3 h intervals. We select the meteorological sites that

have a similar time span to the GPS data and are closest to the GPS site of interest (Figure 1). Information describing these meteorological stations and respective nearby GPS stations are listed in Table S2. The time span for available meteorological records near KULU and KELY is 2000–2010; for QAQ1 and THU3, it is 2003 – 2010; for other GPS stations, it is 2008–2010. In order to compare air temperature with annual uplift variability, we calculate the Annual Mean Surface Air Temperature (AMSAT) and Cumulative Annual Positive Degree Days (CAPDD) per year for each meteorological station. CAPDD may be a better indicator of seasonal, atmospheric-forced melting than AMSAT; on the other hand, AMSAT is a simple indicator of overall climate warming. It is also useful to compare AMSAT with annual mean ocean temperature, discussed later.

2.4. SMB

[12] SMB is the difference between net snow accumulation and net runoff of surface meltwater. Since coastal uplift recorded by GPS is caused by both nearby SMB changes and ice dynamic changes (mainly calving and associated thinning), comparison of the GPS results to SMB changes provides an alternate way to assess atmospheric versus oceanic forcing. We use SMB derived from Regional Atmospheric Climate Model v.2 (RACMO2) [*Ettema et al.*, 2009, 2010a, 2010b; *Kuipers Munneke et al.*, 2011; *van Angelen et al.*, 2012] and calculate SMB in the summertime (June to August) in each year during 2000–2010.

2.5. Sub-surface Ocean Temperature Data and Analysis

[13] Sub-surface water temperature is obtained from the Hadley Center EN3 model output (http://www.metoffice.gov.uk/hadobs/en3/). The EN3 model consists of two products: (1) in-situ sub-surface ocean temperature and salinity profiles with data quality information; and (2) objective analyses using optimal interpolation of the in-situ data profiles with a quality control system [*Ingleby and Huddleston*, 2007]. In this paper, we use the objective analyses product, which contains monthly temperature estimates from 1950 to the present with a spatial resolution of $1° \times 1°$ (about 111 km (N-S) by 38 km (E-W) at 70° north, neat central Greenland) and 42 depth intervals (5 m to 5350 m). Due to the presence of a broad continental shelf, water depth along most of Greenland's coast is limited, which in turn limits the influence of deep water. We

Table 1. Parameters Describing Seasonal Uplift and Atmospheric/Oceanic Condition at KELY, KULU, QAQ1, and THU3

Year	1997	1998	1999	2000	2001	2002	2003	2004	2005	2006	2007	2008	2009	2010
KELY														
Start time (doy)	91±12	139±7	153±8	139±9	169±12	149±15	133±23	106±21	119±40	151±9	134±5	153±28	205±74	108±36
End time (doy)	218±14	356±9	333±9	330±16	357±12	336±30	304±45	259±13	314±29	350±10	288±7	356±21	373±54	335±12
Duration (days)	128±15	217±10	180±9	191±15	188±13	187±28	171±43	153±22	195±37	198±10	154±6	203±29	169±75	228±35
Uplift (mm)	2.9±1.0	10.0±1.3	8.8±1.5	10.3±1.7	7.5±1.6	4.3±1.4	3.4±1.3	3.4±1.1	3.1±1.0	5.6±1.0	7.0±1.0	6.4±2.2	2.1±2.2	14.1±2.5
Uplift rate (*10–2 mm/day)	2.2±0.6	4.6±0.6	4.9±0.8	5.4±0.8	4.0±0.8	2.3±0.7	2.0±0.7	2.2±0.6	1.6±0.5	2.9±0.5	4.5±0.5	3.2±0.4	1.2±0.5	6.2±0.6
AMSAT (°C)	N/D	N/D	N/D	−3.3	−4.3	−5.6	−2.7	−5.0	−2.6	−4.4	−4.2	−4.4	−4.7	−0.2
CAPDD (days)	N/D	N/D	N/D	166	172	155	175	162	161	170	156	163	148	196
AMSSWT (°C)	N/D	N/D	N/D	2.4	2.7	2.3	2.6	2.9	2.8	2.4	2.4	2.5	2.3	3.1
KULU														
Start time (doy)				152±8	144±6	172±11	155±6	140±12	187±9	245±11	188±15	77±10	193±11	172±3
End time (doy)				338±7	322±8	294±10	365±14	396±7	389±9	400±9	315±23	355±4	369±3	356±2
Duration (days)				185±8	177±8	122±33	210±13	255±13	203±10	154±11	127±24	278±11	176±11	185±3
Uplift (mm)				9.9±1.2	7.0±1.1	2.6±0.8	10.3±1.1	7.4±1.0	9.1±1.0	4.5±0.8	1.4±0.8	11.1±0.7	7.2±0.6	14.7±0.7
Uplift rate (*10–2 mm/day)				5.3±0.5	4.0±0.6	2.1±0.5	4.9±0.6	2.9±0.4	4.5±0.5	2.9±0.5	1.1±0.5	4.0±0.3	4.1±0.4	7.9±0.4
AMSAT (°C)				−0.5	−0.5	0.2	1.2	0.1	0.5	−0.5	0.1	−1.4	−1.0	0.5
CAPDD (days)				185	208	203	215	200	184	184	189	155	155	195
AMSSWT (°C)				4.9	5.1	5.0	5.4	5.6	5.5	5.1	5.5	5.5	5.2	5.9
QAQ1*														
Start time (doy)							144±14	192±8	198±7	219±6	194±56	165±37	225+23	165+11
End time (doy)							336±19	376±9	404±5	384±6	298±65	350±19	384+13	370+8
Duration (days)							192±18	183±9	206±7	165±7	101±40	185±36	159±21	204±12
Uplift (mm)							4.6±0.9	6.8±0.8	8.3±0.8	5.8±0.7	0.6±0.4	3.6±1.6	5.1±1.5	12.4±1.7
Uplift rate (*10–2 mm/day)							2.4±0.5	3.7±0.4	4.0±0.4	3.5±0.4	0.5±0.3	1.9±0.4	3.2±0.4	6.1±0.4
AMSAT (°C)							2.6	2.1	2.6	1.6	2.0	0.5	1.4	4.6
CAPDD (days)							240	242	258	215	229	219	194	272
AMSSWT (°C)							4.9	4.9	4.8	4.7	4.6	4.6	4.3	4.9
THU3*														
Start time (doy)							161±20	330±30	154±7	185±24	149±11	76±277	218±37	211±16
End time (doy)							377±10	426±9	392±7	384±11	420±126	367±29	398±23	350±11
Duration (days)							217±20	97±32	238±9	194±32	268±125	333±257	184±36	139±16
Uplift (mm)							5.1±1.0	1.3±0.6	6.0±0.9	1.4±0.8	2.5±1.4	3.5±3.4	5.6±2.0	5.7±1.9
Uplift rate (*10–2 mm/day)							2.4±0.5	1.3±0.5	2.5±0.4	0.7±0.4	0.9±0.3	1.2±0.3	3.1±0.4	4.1±0.5
AMSAT (°C)							−7.8	−9.6	−8.7	N/D	−8.5	−9.2	−9.0	−6.8
CAPDD (days)							117	113	119	N/D	103	113	107	116
AMSSWT (°C)							0.3	0.3	0.3	0.4	0.4	0.3	0.1	0.2

Note: Uncertainty is defined at the 68% confidence interval (Supplemental information). Units for start time and end time are day of year (doy). End times exceeding 365/366 indicate that seasonal uplift continues to the following year. N/D – no data.

looked at data in the EN3 model from 5 m to 447 m depth (depth levels 1 to 22), selecting 14 "voxels" (model volume elements) that are close to our GPS stations (Figure 1). To compare sub-surface water temperature with annual uplift and atmospheric mean temperature, we calculate the Annual Mean Sub-Surface Water Temperature (AMSSWT) averaged over this upper 442 m of ocean depth range. The deeper parts of this water volume will not necessarily interact with all outlet glaciers due to topographic barriers near a given fjord entrance (usually end moraines from the Last Glacial Maximum at about 22 ka) and circulation complexities. We have not accounted for such local effects in our analysis.

3. Results

3.1. Seasonal Uplift/Subsidence Pattern

[14] Figure 3 and Table 1 show the five parameters estimated from the GPS time series for the four time series that exceed 5 years (QAQ1, KULU, KELY, and THU3). For KULU, data in the early part of 2008 is missing; thus, the estimate of start time in 2008, end time in 2007, and duration and uplift both in 2007 and 2008 are less reliable.

[15] The distance between a given GPS site and the locus of nearby mass loss will affect the magnitude of observed uplift. For example, site HEL2 is located very close (less than 5 km) to the terminal region of Helheim, a large outlet glacier in southeast Greenland, and experienced 19 mm uplift in the summer of 2010, one of the largest values observed in our study. We estimated distance to the nearest glacier front for the various stations (Table 2) but note that in some cases, the distance is ambiguous, since more than one nearby outlet glacier may be influencing measured uplift. For this reason, direct comparison of uplift magnitude may not be useful. However, a comparison of year-to-year changes for a given site will be useful because over short (several year) time scales, because the distance change effects are small. For longer (decadal scale and longer) periods, this could become an issue at locations with rapidly retreating ice margins unless sites can be periodically relocated.

[16] In 2010, the beginning of the uplift season for QAQ1, KULU, and KELY was much earlier than previous years (QAQ1: 25 days earlier than the 2003–2009 average; KELY: 34 days earlier than the 1997 – 2009 average; KULU: 59 days earlier than the 2000 – 2009 average). Note that when calculating these average values, we do not include

parameter estimates with significant uncertainties. For example, the anomalous negative duration with large uncertainty for KULU at 2007 is ignored in KULU's average.

[17] In contrast to QAQ1, KULU, and KELY, site THU3 began uplifting 23 days later than the 2003 – 2009 average. For KELY, the end of the uplift season was 14 days later in 2010 (KULU: 13 days later than the 2003–2009 average; KELY: 14 days later than the 1997 – 2009 average). For QAQ1, uplift ended in 2010 about the same day as the previous mean value. However, for KULU and THU3, uplift ended earlier in 2010 (KULU: 13 days earlier; THU3: 49 days earlier). Hence, for QAQ, KULU, and KELY, the duration of summer uplift (and presumably melting) was somewhat longer in 2010 (QAQ1: 23 days; KULU: 46 days; KELY: 48 days) than the average of previous years. For THU3, the duration is about 46 days shorter than the average.

[18] The amount of uplift in 2010 for three sites (QAQ1, KULU, and KELY) in south Greenland exceeded 10 mm and was larger than in the previous years, implying an increase of ice mass loss in 2010 at these locations, which agrees well with the positive 2010 uplift anomaly in south Greenland observed by *Bevis et al.* [2012]. No significant change in uplift occurred at northwest site THU3 in 2010. Our analysis differs slightly from that of *Bevis et al.* [2012] who report a negative 2010 uplift anomaly in northwest Greenland; our data suggest 2010 uplift at site THU3 is about the same level as the previous year (Figures 3 and 5). In agreement with recent GRACE results [*Schrama and Wouters*, 2011; *Chen et al.*, 2011; *Khan et al.*, 2010], our data show decreased uplift for sites KULU and QAQ1 in south Greenland in 2007 and increased uplift for site THU3 in northwest Greenland from 2007 to 2009. Uplift correlated strongly ($R > =0.5$, where R is the correlation coefficient) and significantly ($P < =0.05$, where P is the significance probability) with duration for sites in southern coastal Greenland, indicating that the length of summer melting influences the amount of summer melting in that area (Figure 4). In addition, the speed of summer uplift in 2010 for most sites was significantly faster than previous years, implying more intense summer melting. From these observations, we can infer that for most of southern coastal Greenland, the anomalously high melting in 2010 reflected both a longer duration melting season and more intense melting.

[19] We also analyzed data from 14 sites with shorter time spans, May 2008 to May 2011, covering the 2008, 2009, and 2010 melt seasons (Figure 5). For most sites in southern Greenland, the largest
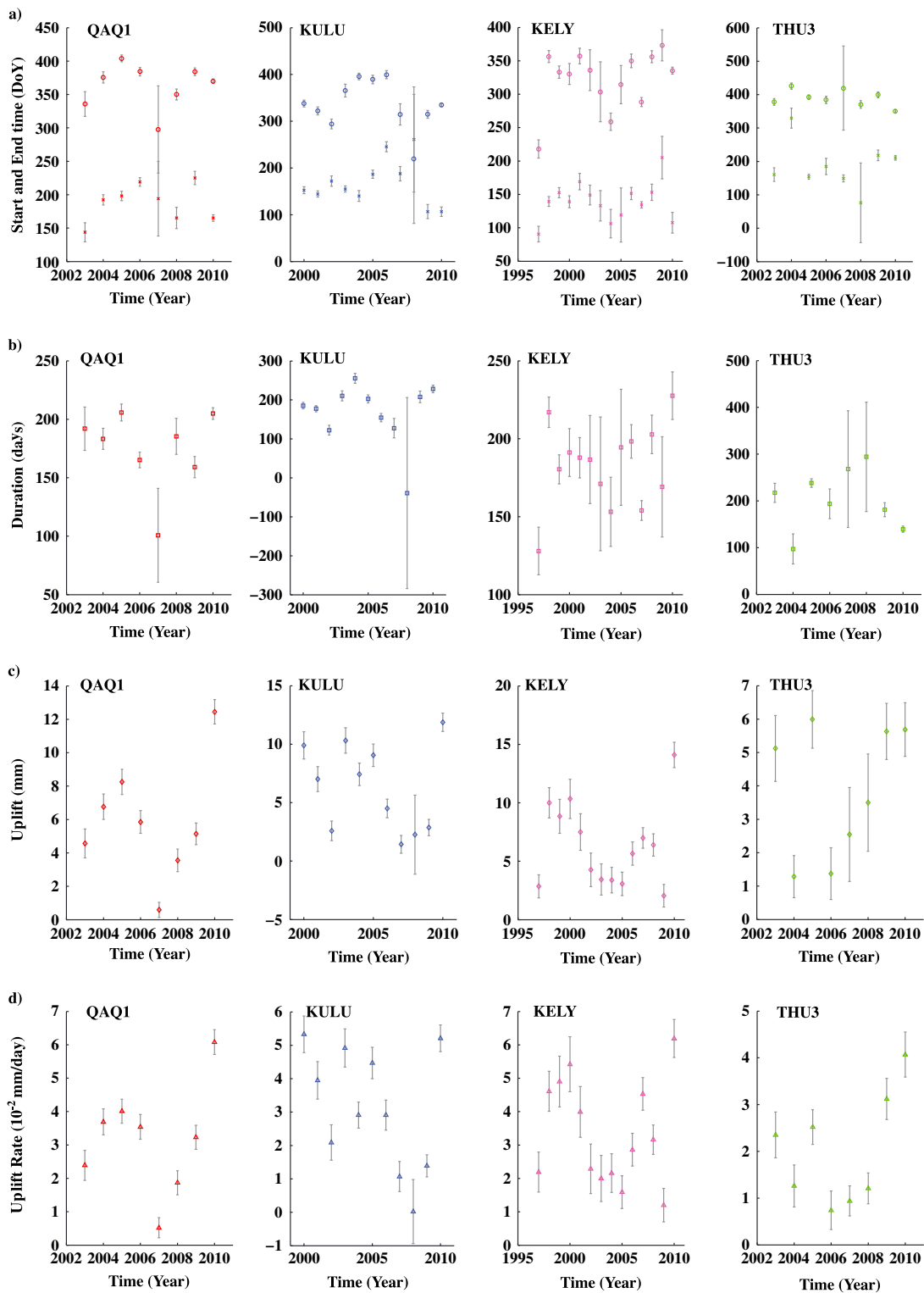
Figure 3. Annual variations of the five parameters defining seasonal uplift calculated for the four sites with longest observation record (red circles in Figure 1). (a) Uplift start time (cross) and end time (circle), (b) uplift duration, (c) uplift magnitude, and (d) uplift rate. Gray line represents uncertainty.

Table 2. Recent Uplift History and Glacier Proximity for All GPS Sites Considered in This Study

| Site | Glacier | Distance (km) | Uplift(mm) | | | 2010 Uplift Increase(%) | |
			2008	2009	2010	2010/2008	2010/2009
DKSG	M	5	5.2 ± 0.8	8.3 ± 0.7	8.1 ± 1.0	35.8 ± 12.7	-2.5 ± 15.3
HEL2	M	3	12.2 ± 0.7	9.0 ± 0.7	19.0 ± 0.7	35.80 ± 4.4	52.6 ± 4.1
HJOR	M	15	12.5 ± 0.7	7.0 ± 0.6	18.3 ± 0.7	31.7 ± 4.6	61.7 ± 3.6
KAGA	M	7	7.6 ± 0.7	8.3 ± 0.7	16.7 ± 0.8	54.5 ± 4.7	50.3 ± 4.8
KELY	L	30	6.4 ± 1.0	2.1 ± 1.0	14.1 ± 1.1	54.6 ± 7.9	85.1 ± 7.2
KSNB	M	50	9.6 ± 0.8	7.6 ± 0.6	12 ± 0.8	20.0 ± 8.5	36.7 ± 6.5
KULL	M	25	6.0 ± 0.7	8.5 ± 0.7	6.5 ± 0.7	7.7 ± 14.7	-30.8 ± 17.7
KULU	M	50	2.3 ± 3.4	2.9 ± 0.7	11.9 ± 0.8	80.7 ± 28.6	75.6 ± 6.1
LYNS	M	20	11.1 ± 0.7	7.2 ± 0.6	14.1 ± 0.7	21.3 ± 6.3	48.9 ± 5.0
MARG	M	2	4.6 ± 0.9	7.2 ± 0.7	6.9 ± 0.8	33.3 ± 15.2	-4.3 ± 15.8
PLPK	M	2	9.8 ± 0.8	5.8 ± 0.7	14.2 ± 1.0	31.0 ± 7.4	59.2 ± 5.7
QAQ1	M/L	50/45	3.6 ± 0.7	5.1 ± 0.6	12.4 ± 0.7	71.0 ± 5.9	58.9 ± 5.4
RINK	M	7	6.9 ± 0.8	7.3 ± 0.7	10.0 ± 0.8	31.0 ± 9.7	27.0 ± 9.1
SENU	M/L	12/3	N/D	11.5 ± 0.6	19.3 ± 0.7	N/D	40.4 ± 3.8
SRMP	M	2	6.9 ± 0.7	7.7 ± 0.7	11.6 ± 0.8	40.5 ± 7.3	33.6 ± 7.6
THU3	M	25	3.5 ± 1.5	5.6 ± 0.8	5.7 ± 0.8	38.6 ± 27.7	1.8 ± 19.6
TIMM	M	35	10.4 ± 0.7	8.4 ± 0.7	13.7 ± 0.7	24.1 ± 6.4	38.7 ± 6.0
TREO	M	9	14.7 ± 0.7	5.4 ± 0.6	17.6 ± 0.8	16.5 ± 5.5	69.3 ± 3.7

Note: M represents marine-terminating glacier, L represents land-terminating glacier. Percentage differences between uplift in 2010 and uplift in two earlier years are shown in last two columns.

uplift occurred in 2010, followed by 2008, with 2009 having the smallest uplift. However, sites in northern Greenland (KULL, DKSG, THU3, and MARG) did not experience significant uplift variation from 2008 to 2010, perhaps indicating less sensitivity to short-term variations in forcing. Uplift in 2009 was somewhat higher than the other 2 years for most sites in northern Greenland. On average, the annual uplift in southern Greenland is higher than that in northern Greenland, especially in 2010.

3.2. Air Temperature Analysis

[20] Figure 6 shows time series of the two atmospheric parameters for the four meteorological stations closest to QAQ1, KULU, KELY, and THU3, the sites with the longest GPS time series. 2010 AMSAT at KELY was nearly 4°C above the 2000 – 2009 mean. For QAQ1, THU3, and KULU, the differences between the 2010 AMSAT and the means of their base periods are 2.8°C, 2.0°C, and 1.0°C,
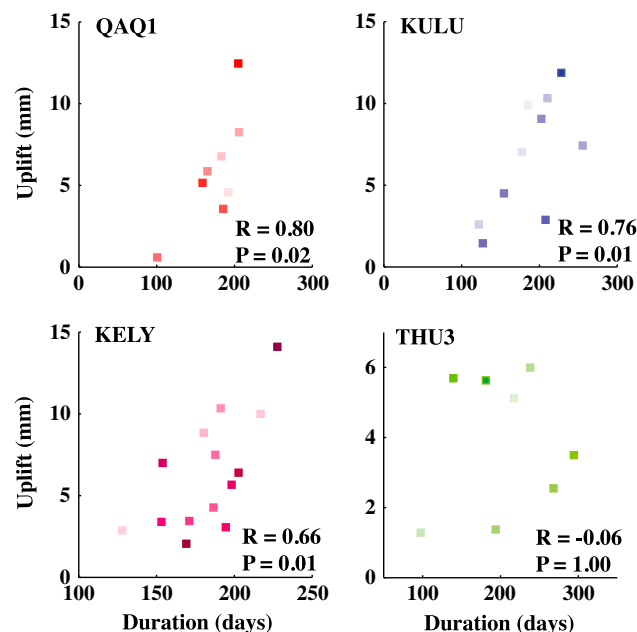
Figure 4. Uplift versus duration for the four sites with longest observation record. Colors varying from light to dark represent data from earlier to more recent.
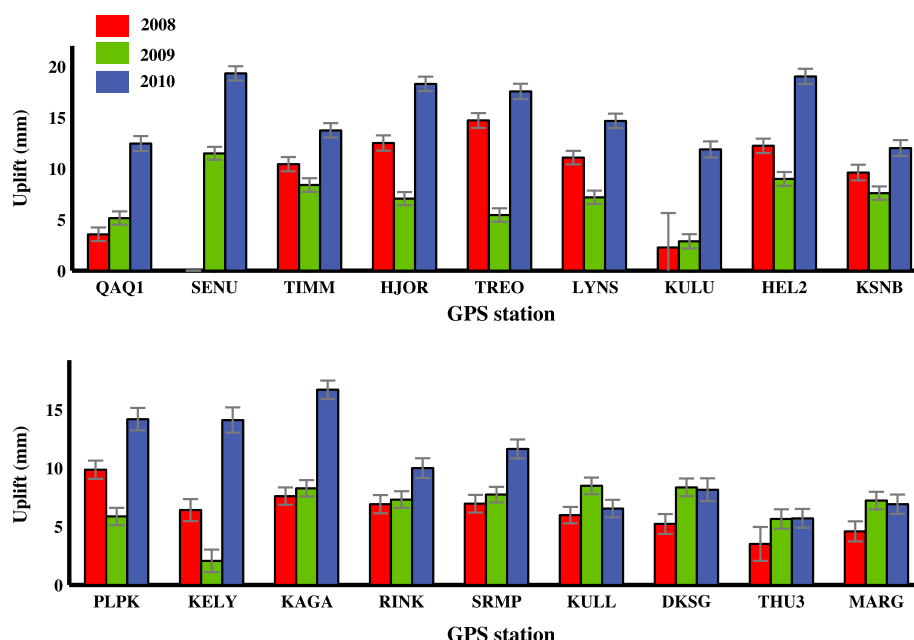
Figure 5. Seasonal uplift patterns for 2008–2010. GPS sites are ordered by latitude, from south to north. Note change between KAGA (69.2°N) and RINK (71.9°N) with lower amplitude and lower variability uplift at the more northern sites.

respectively (Table 1 and Figure 6a). CAPDD provides an index of surface melting duration, for comparison with the duration of uplift. In 2010, all four sites experienced a longer CAPDD compared to previous years, although the difference was small at THU3 in northwest Greenland (Table 1 and Figure 6b). For QAQ1, there was a dramatic increase in CAPDD for 2010 compared to earlier years. We also observe the expected latitudinal pattern in both atmospheric indices, with southern sites experiencing higher AMSAT and longer CAPDD compared to northern sites.

3.3. Comparison to SMB

[21] We compare our GPS observation to SMB derived from RACMO2 [*Ettema et al.*, 2009, 2010a, 2010b]. Figure 7 shows the difference between Greenland ice sheet SMB in the summertime (June to August) of 2010 and individual years of the previous decade. SMB in summer 2010 was more negative than previous years in Greenland's southern coastal areas, indicating significant surface mass loss at that time. However, the pattern in northwest Greenland is somewhat different. While coastal SMB was negative in both 2009 and 2010 (significant summer melting), it was somewhat less negative in 2010, so that the difference (2010–2009) is slightly positive (Figure 7). GRACE data actually suggests slight mass gains in the interior [*Bevis et al.*, 2012]. We see seasonal uplift at all northwest Greenland sites (Figure 5) while at site THU3,

summer 2010 uplift is both high (Figure 3c) and intense (i.e., high rate, Figure 3d), which does not reconcile with the SMB model. Perhaps, oceanic forcing or dynamical changes (thinning from longer-term climate trends) are responsible for some of the coastal mass loss here, by definition not part of the SMB model, and not sensed by the lower spatial resolution of GRACE. These possibilities are discussed in more detail below.

3.4. Sub-Surface Ocean Temperature Analysis

[22] Figure 8 shows the differences between AMSSWT in 2010 and previous years (2000 to 2009) for Greenland's coastal areas. Sub-surface ocean temperature in 2010 is significantly higher than previous years near both southeast and southwest Greenland. However, northwest Greenland in 2010 does not experience this temperature anomaly. Figure 9 shows time series of AMSSWT obtained from voxels near respective GPS stations for the period 2000–2010. As in Figure 8, high temperature was observed in 2010 compared with the previous decade. In addition, the spatial variations of AMSSWT can be clearly seen: AMSSWT reaches its maximum in southeast Greenland and decreases to southwest Greenland, further decreasing in northwest Greenland.

3.5. Correlation Analysis

[23] We now investigate a series of correlations between uplift and atmospheric or oceanic parameters,
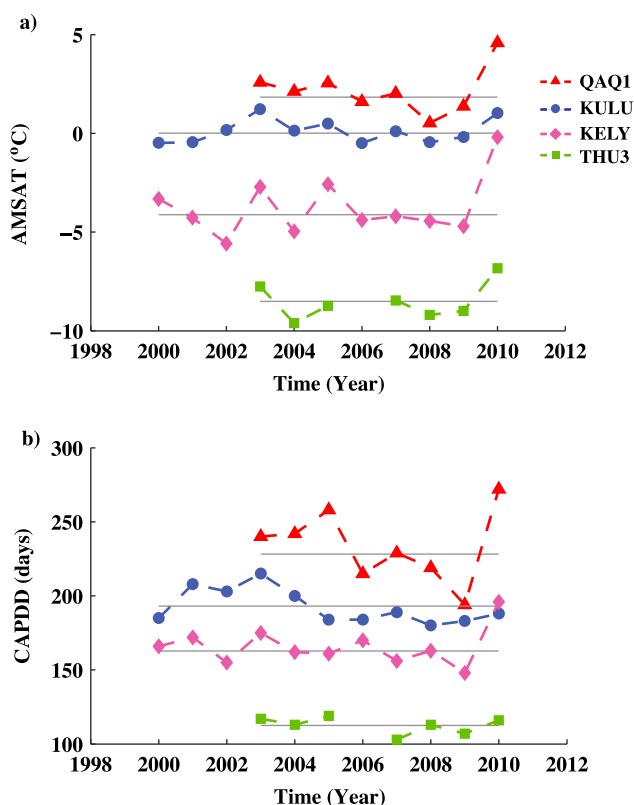
Figure 6. (a) AMSAT (Annual mean surface air temperature). (b) CAPDD (Cumulative annual positive degree days) for the four GPS stations with longest observation record. Solid gray line represents the mean value of reference period.
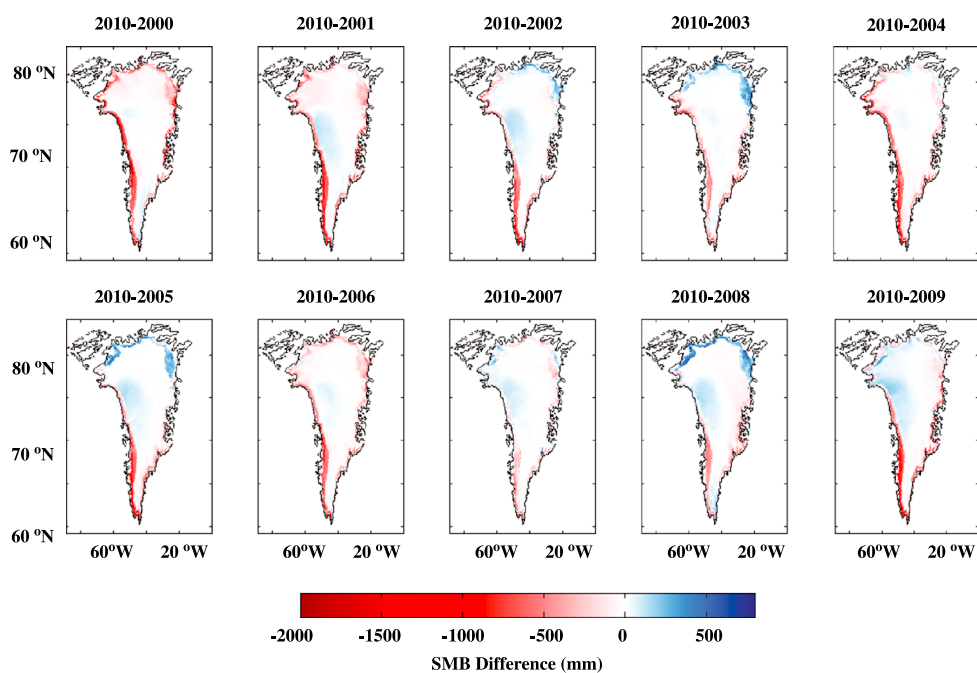
Figure 7. Difference of Surface Mass Balance (SMB model from RACMO2) in summertime (June to August) between 2010 and 20XX (XX = 00–09) for the Greenland region. Red color indicates that 2010 had a relatively negative SMB (more surface mass loss or less surface mass gain) compared to previous years, and blue color indicates that 2010 had a relatively positive SMB (less surface mass loss or more surface mass gain) compared to previous years.
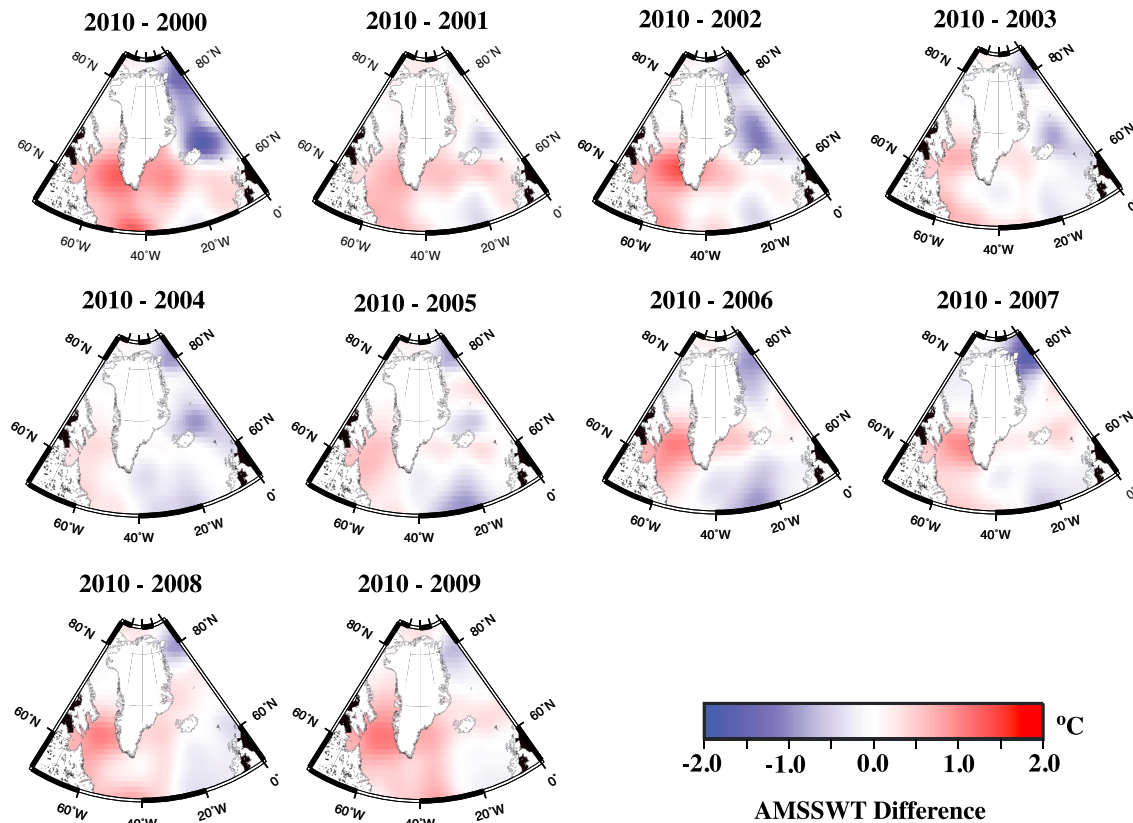
Figure 8. Difference of AMSSWT (Annual mean, sub-surface water temperature, depth range 5 m – 447 m) between 2010 and 20XX (XX = 00–09) for the Greenland region. Warmer colors indicate that 2010 was warmer the previous year at a given location.

in particular looking for short-term (several year) linear relations between forcing and response. Since glacier dynamics (a possible influence on coastal mass loss and uplift) can be highly non-linear, with response times exceeding decades, we may be able to infer its influence indirectly by investigating conditions where correlations between the simple forcing functions described here (atmospheric or ocean temperature) are not observed.

3.5.1. Uplift and Atmospheric Factors

[24] To investigate the possible relationship between air surface temperature and seasonal uplift pattern, we first look at data for sites with more than 5 years of GPS data. We looked at correlations between uplift and atmospheric parameters, with uplift weighted by its uncertainty. We assess a correlation to be good when the correlation is both strong (correlation coefficient $R > =0.5$) and significant ($P < =0.05$). Uplift duration and CAPDD are not well correlated (Figure 10), implying a role for ocean forcing for at least some sites. Figure 11 investigates correlations between the magnitude of annual

uplift, AMSAT, and CAPDD. Both AMSAT and CAPDD show good correlation with seasonal uplift at KELY and QAQ1. However, uplift and the atmospheric parameters are not well correlated at THU3, and CAPDD is not well correlated with uplift at KULU.

[25] We can use the larger GPS dataset to investigate possible relationships between seasonal uplift and AMSAT and CAPDD for the years 2008 – 2010 by looking at the pattern of variation (Figure 12). Poor agreement between uplift and the two atmospheric parameters is observed at most sites, except for KELY. Moderate agreements between uplift and either AMSAT or CAPDD are observed for QAQ1, KAGA, SRMP, and RINK.

[26] The larger GPS dataset can also be used to investigate possible temporal variations in the relationship between seasonal uplift and AMSAT, CAPDD for 2008–2010 (Figure 13). 2010 uplift shows stronger correlations with both local AMSAT and CAPDD compared to previous years. 2009 exhibits especially poor correlation between uplift and the local atmospheric parameters.
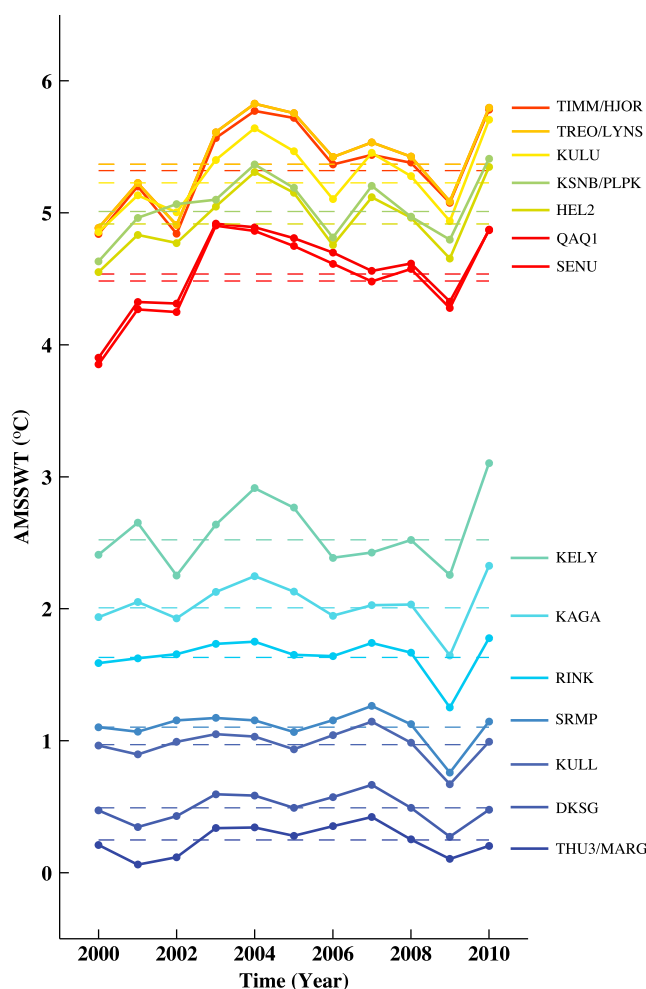
Figure 9. AMSSWT (Figure 8) for "voxels" (model volume elements) nearest a given GPS station. Warmer colors indicate southern latitudes, cooler colors indicate northern latitudes. Dashed color line represents 2000–2009 means. Note the pronounced 2010 anomaly for most locations, decreasing in intensity to the north.

3.5.2. Uplift and Ocean Warming

[27] As with the correlation analysis between seasonal uplift and atmospheric parameters, we first look at the correlation between seasonal uplift and AMSSWT for sites with more than 5 years of GPS data (Figure 11c). Seasonal uplift and AMSSWT are well correlated only for KELY over this longer time period. Strong negative correlation between uplift and AMSSWT is observed at THU3. However, when we look at the larger GPS data set for shorter 2008 – 2010 period (Figure 12), a different pattern emerges. Seasonal uplift has a pattern similar to AMSSWT for most sites in southern Greenland. For example, compare the uplift pattern to AMSSWT for these 3 years at the seven adjacent sites TIMM, HJOR, TREO, LYNS, HEL2, KSNB, and PLPK in southeast Greenland (Figure 12). The temporal variation in uplift closely

matches trends in the ocean parameter (AMSSWT) but is only in moderate agreement with the atmospheric parameters (AMSAT and CAPDD). However, this pattern breaks down for sites in northwest Greenland (Figure 12). Figure 13 suggests that 2010 uplift is somewhat better correlated with AMSSWT than CAPDD, although the differences are small. Nevertheless, these results suggest an important role for oceanic forcing in the 2010 melt anomaly, especially for southern sites. As with the atmospheric parameters, uplift correlates poorly with AMSSWT in 2009, when uplift is small at many sites (Figure 5).

3.6. Uplift Acceleration

[28] The spatial gradients for air and sub-surface water temperature differ: surface air temperature decreases from south to north, while sub-surface
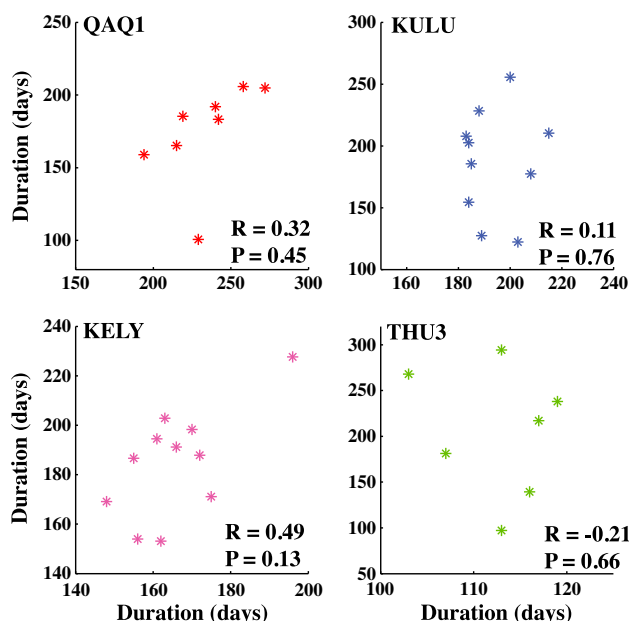
**Figure 10.** Uplift duration versus CAPDD (Figure 6).

water temperature decreases clockwise around Greenland from southeast to northwest, following the path of the Irminger Current (IC) (Figures 6 and 9). Hence, it may be possible to estimate the relative influence of air and ocean forcing on the 2010 uplift anomaly by looking at spatial variations in the short-term changes (acceleration) of uplift.
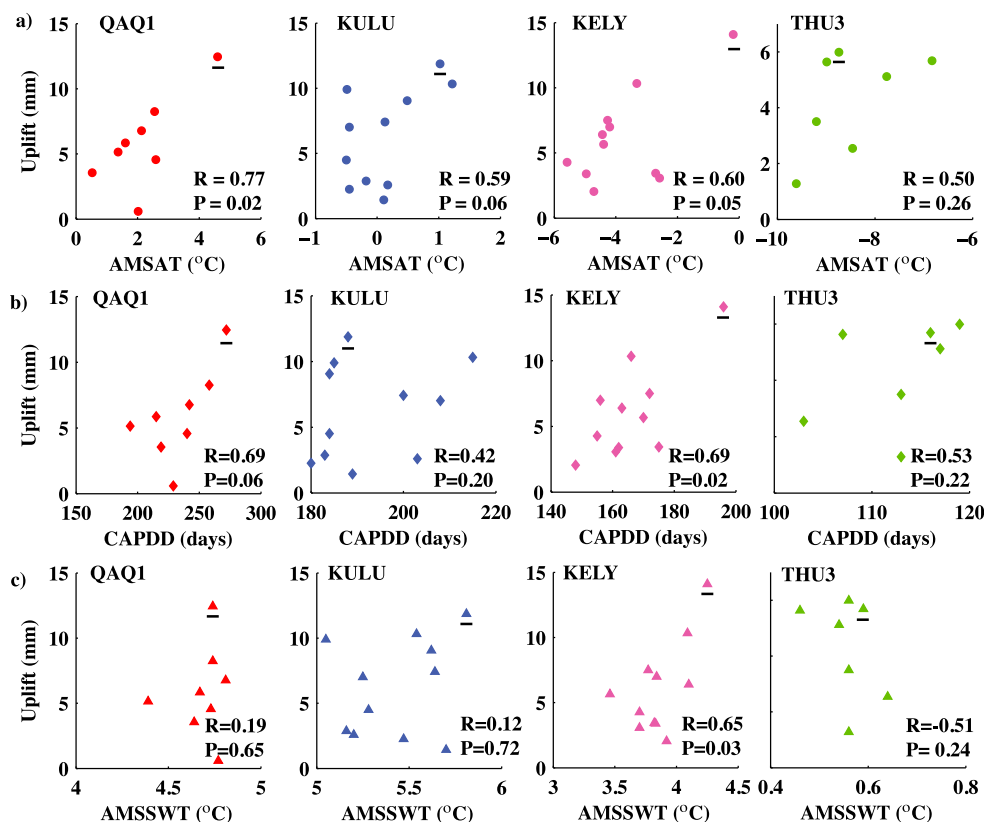
Figure 11. Spatial variation of seasonal uplift for four stations with longest time span related to (a) AMSAT (Figure 6); (b) CAPDD (Figure 6); and (c) AMSSWT (Figure 8). Underlined symbol is 2010.
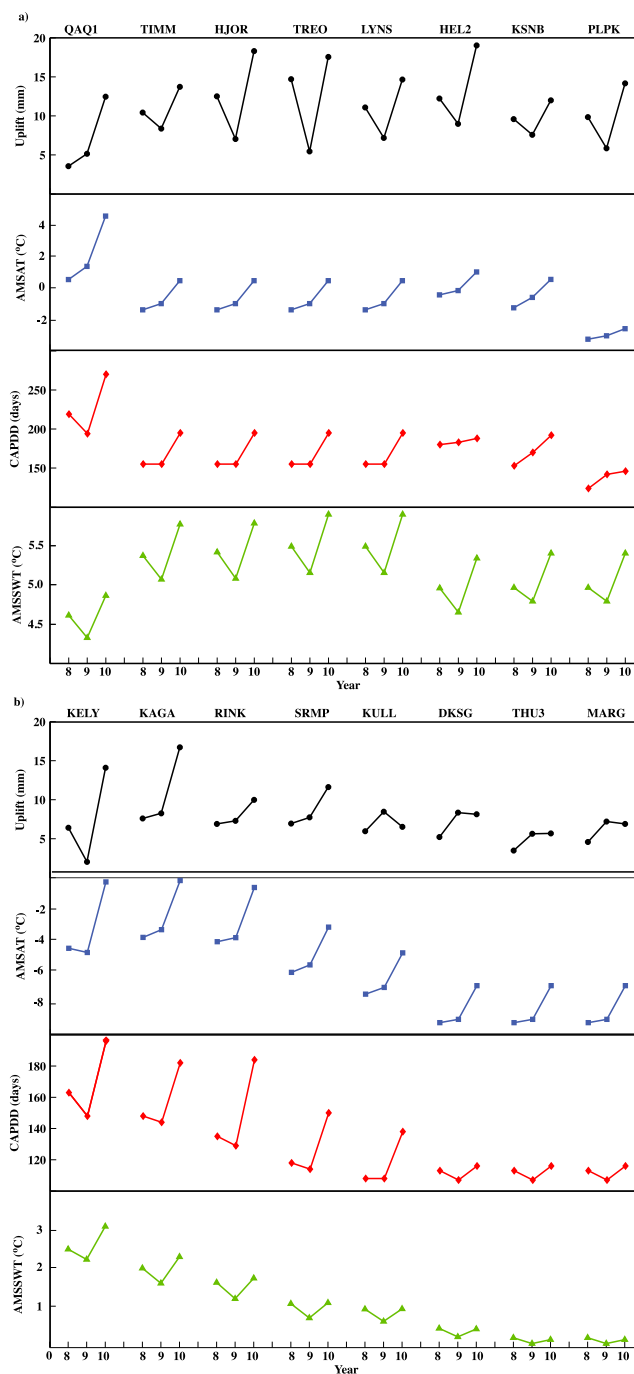
Figure 12. Comparison between seasonal uplift patterns and atmospheric parameters (AMSAT and CAPDD, Figure 6) as well as the ocean temperature parameter (AMSSWT, Figure 8) for 2008–2010. Uplift pattern as shown in Figure 5. SENU and KULU are eliminated here due to lack of data in 2008. GPS stations are ordered from south to north.

[29] Acceleration of vertical crustal motion was estimated from the GPS time series by fitting a constant acceleration model, following *Jiang et al.* [2010]. Here, we focus on two time scales, the mid-2007 to early 2011 period for all available stations, and the decadal (or longer) time series available for four stations.

[30] Figure 14 compares the uplift acceleration of 17 GPS sites (between mid-2007 and early 2011) and both atmospheric and oceanic parameters in 2010. Although there are relatively good correlations between acceleration and two atmospheric parameters (AMSAT and CAPDD), the strongest correlation is with AMSSWT. Also, the largest acceleration
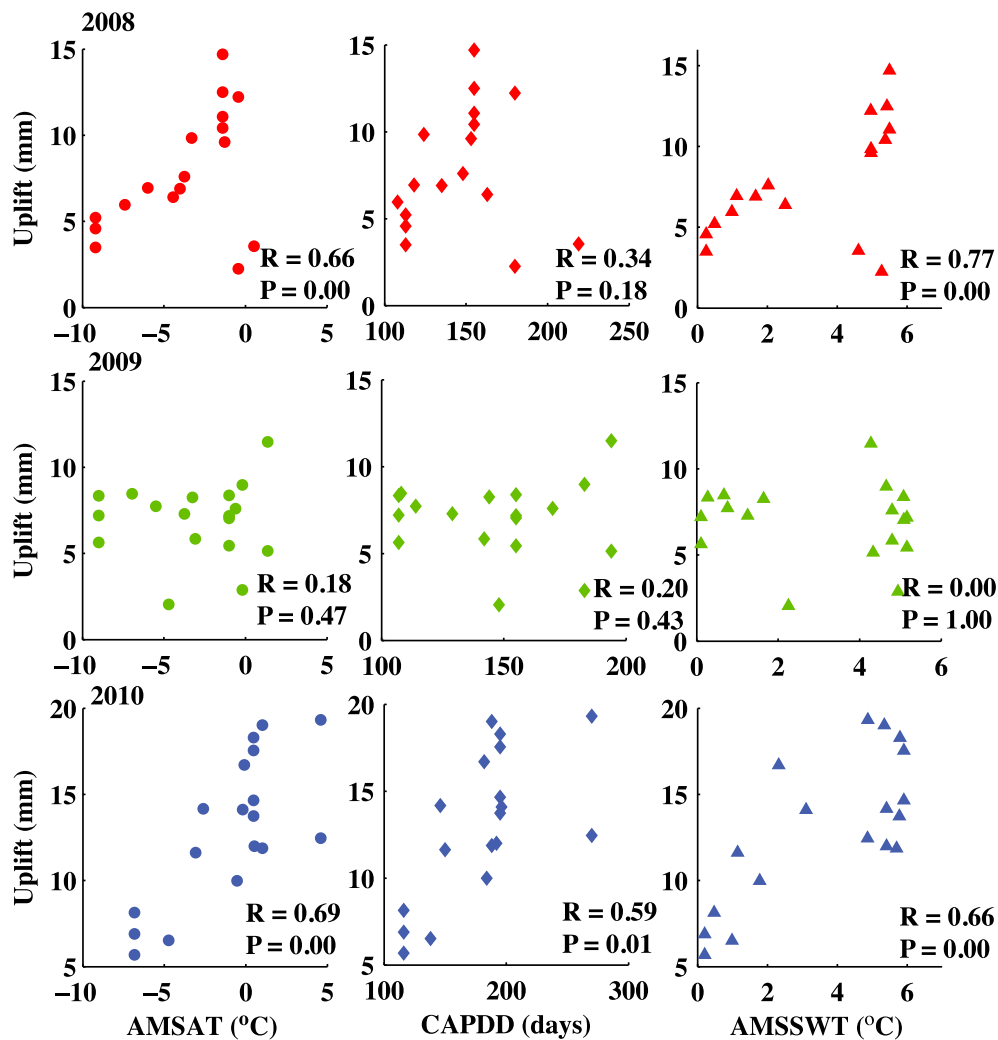
Figure 13. Temporal variation of seasonal uplift for all stations for 2008–2010 as a function of (a) AMSAT (Figure 6), (b) CAPDD (Figure 6), and (c) AMSSWT(Figure 8).

occurs at site PLPK in southeast Greenland rather than the southernmost site QAQ1. QAQ1 had the highest temperature and longest CAPDD in 2010, yet did not experience the largest uplift anomaly in that year. This suggests that atmospheric temperature is not the dominant factor causing the difference in accelerations. Site PLPK is located close to where the IC first approaches the coast of Greenland (Figure 1). Hence, the observed uplift acceleration in 2010 may reflect the influence of warm Irminger Water (IW), through its melting of sub-surface ice in marine-terminating glaciers [*Holland et al.*, 2008; *Straneo et al.*, 2010, 2012].

[31] During the period mid-2007 to early 2011, all sites in south and central Greenland show positive accelerations, with the highest accelerations recorded at sites in southeast Greenland. In contrast, sites in northwest Greenland show negative acceleration

(Figure 14 and Table 3a). This marks a significant change from our earlier study [*Jiang et al.*, 2010] which showed accelerating uplift in northwest Greenland up until 2008. Comparing with the result of *Jiang* et al. [2010], our data show higher accelerations for sites in south Greenland until May 2011, reflecting the enhanced 2010 uplift. Figure 15 shows the relative difference between uplift in 2010 compared to 2008 and 2009. Over this period, uplift (and presumably mass loss) increases in southern Greenland, but decreases or is essentially unchanged in northwest Greenland.

3.7. Comparison to GRACE

[32] Our GPS data are in agreement with GRACE observations showing significant anomalous mass loss in southern Greenland in 2010, as observed
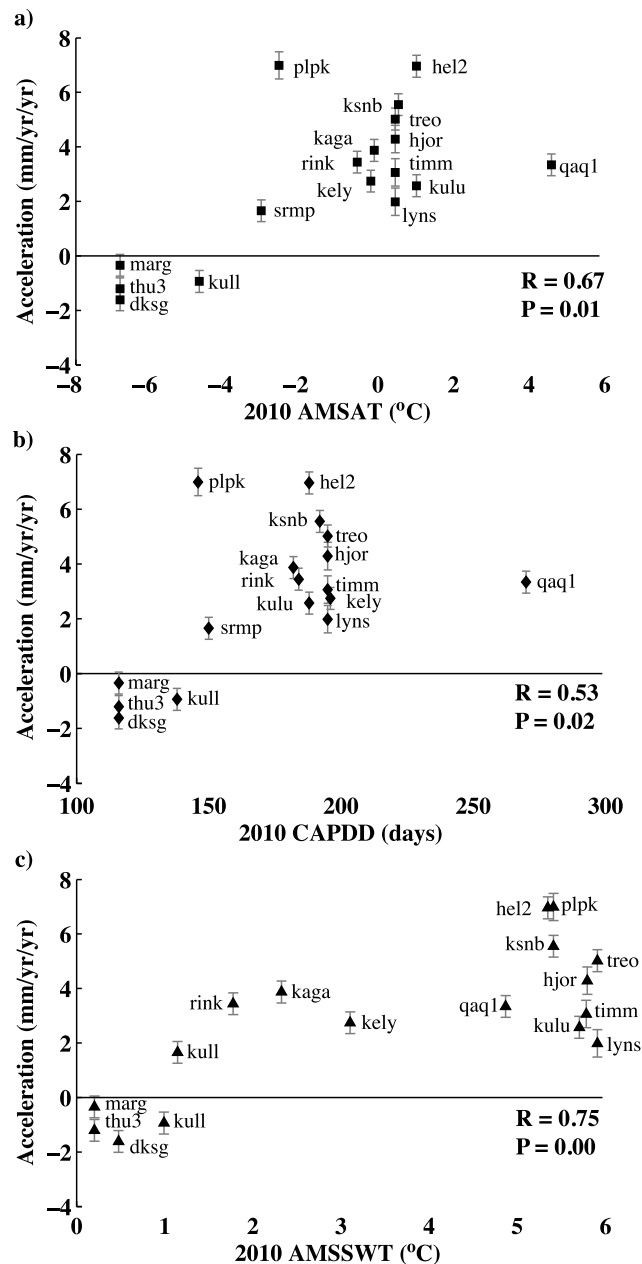
Figure 14. Spatial variation of uplift accelerations as a function of (a) AMSAT (Figure 6), (b) CAPDD (Figure 6), and (c) AMSSWT (Figure 8) of 2010.

by *Bevis et al.* [2012]. However, we do not observe mass gain in northern Greenland suggested by the GRACE observations. As pointed out by *Bevis et al.* [2012], this difference likely reflects the spatial resolution of GRACE, giving this sensor sensitivity to mass gain in the interior of Greenland (to which coastal GPS would not be sensitive) and perhaps sensitivity to mass changes on the other side of Baffin Bay (Devon, Ellesmere Islands).

[33] It is also useful to compare our GPS results with GRACE over various time spans. Accelerations of

the four GPS time series with longer time spans are shown in Table 3b. From 2007 to 2009, ice loss slowed down in the southeast and sped up in the northwest [*Schrama and Wouters*, 2011; *Chen et al.*, 2011; *Khan et al.*, 2010], while the new GPS data detected acceleration beginning again in the south Greenland with the intense 2010 melt season. Thus, the positive accelerations in southeast Greenland and negative or zero accelerations in northwest Greenland between middle 2007 and early 2011 are dominated by variations of mass loss in the summer of 2010.

Table 3. GPS Uplift Data Fit to a Model of Constant Acceleration

(a) Site	Latitude (deg N)	Longitude (deg E)	Tstart (year)	Tstop (year)	N (Day)	V_0 (mm/yr)	Acceleration (mm/yr/yr)	Amp (mm)	RMS (mm)
DKSG	76.35	−61.67	2007.64	2011.39	1263	21.3 ± 0.8	−1.6 ± 0.4	4.3	7.4
HEL2	66.40	−38.22	2007.65	2011.39	1324	4.3 ± 0.8	6.9 ± 0.4	8.1	7.4
HJOR	63.42	−41.15	2007.62	2011.39	1134	1.1 ± 0.9	4.3 ± 0.5	7.4	7.9
KAGA	69.22	−49.81	2007.36	2011.39	1418	11.1 ± 0.9	4.3 ± 0.4	6.5	8.1
KELY	66.99	−50.94	2007.64	2011.39	1062	0.0 ± 0.9	2.7 ± 0.4	4.9	7.2
KSNB	66.86	−35.58	2007.64	2011.39	1271	2.2 ± 0.7	5.5 ± 0.4	5.1	6.9
KULL	74.58	−57.23	2007.62	2011.39	1311	12.2 ± 0.8	−0.9 ± 0.4	3.9	7.4
KULU	65.58	−37.15	2007.61	2011.39	1171	4.9 ± 0.8	2.6 ± 0.4	3.7	7.2
LYNS	64.43	−40.20	2007.66	2011.39	1341	7.1 ± 0.9	2.0 ± 0.5	5.4	8.5
MARG	77.19	−65.69	2007.67	2011.39	1349	10.8 ± 0.8	−0.3 ± 0.4	2.9	7.8
PLPK	66.90	−34.03	2007.61	2011.18	1235	−1.3 ± 0.8	7.0 ± 0.5	4.8	7.4
QAQ1	60.72	−46.05	2007.65	2011.39	1250	−0.9 ± 0.8	3.3 ± 0.4	3.7	7.0
RINK	71.85	−50.99	2007.67	2011.39	1346	4.2 ± 0.8	3.4 ± 0.4	4.7	7.9
SENU	61.07	−54.39	2008.38	2011.39	1053	−5.4 ± 1.0	11.8 ± 0.6	11.5	6.9
SRMP	72.91	−47.14	2007.62	2011.39	1365	15.1 ± 0.7	1.6 ± 0.4	4.7	7.4
THU3	76.54	−68.83	2007.64	2011.39	1195	11.0 ± 0.8	−1.2 ± 0.4	2.6	7.8
TIMM	62.54	−42.29	2007.65	2011.28	1115	3.1 ± 1.0	3.1 ± 0.5	6.6	8.7
TREO	64.28	−41.38	2007.67	2011.39	1273	1.6 ± 0.9	5.0 ± 0.4	6.4	8.2
(b) KELY	66.99	−50.94	1996.04	2011.39	4564	−3.2 ± 0.1	0.6 ± 0.1	3.8	7.5
KULU	65.58	−37.15	1999.88	2011.39	3696	3.5 ± 0.2	0.8 ± 0.1	3.8	8.3
QAQ1	60.72	−46.05	2002.39	2011.39	3034	1.8 ± 0.3	0.5 ± 0.1	3.5	6.9
THU3	76.54	−68.83	2002.40	2011.39	3017	4.5 ± 0.4	0.7 ± 0.1	1.9	7.8

*$T_{start, end}$: start and end time of GPS time series, in years.

N: number of days of data in GPS time series. Amp: amplitude of annual variation.

RMS: root mean square misfit of the constant acceleration model to the time series.

V_0: vertical velocity at the beginning of the time series.

[34] In terms of annual variations, *Wouters et al.* [2008] detected large mass loss along the coasts of southeastern and northwestern Greenland in the summers of 2003, 2005, and 2007. Our data show high uplift at northwest and southeast GPS site in 2003 and 2005 but not in 2007. The different spatial scales of GPS and GRACE could cause this difference.

4. Discussion

[35] Seasonal uplift in coastal Greenland, as measured by high precision GPS and our cubic spline time series model, shows considerable site-to-site and year-to-year variation, which we believe correlates with variations in the mass loss of nearby outlet
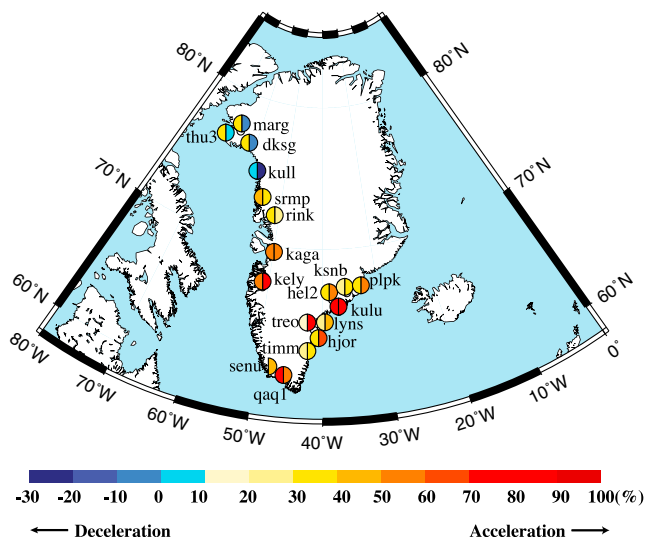
Figure 15. Site map of relative difference between uplift in 2010 and uplift in 2008 and 2009. The left half circle shows percentage difference between the uplift in 2008 and 2010: $\Delta U_{10/08} = (U_{10} - U_{08})/U_{10}$; right half circle shows percentage difference between uplift in 2009 and 2010: $\Delta U_{10/09} = (U_{10} - U_{09})/U_{10}$.
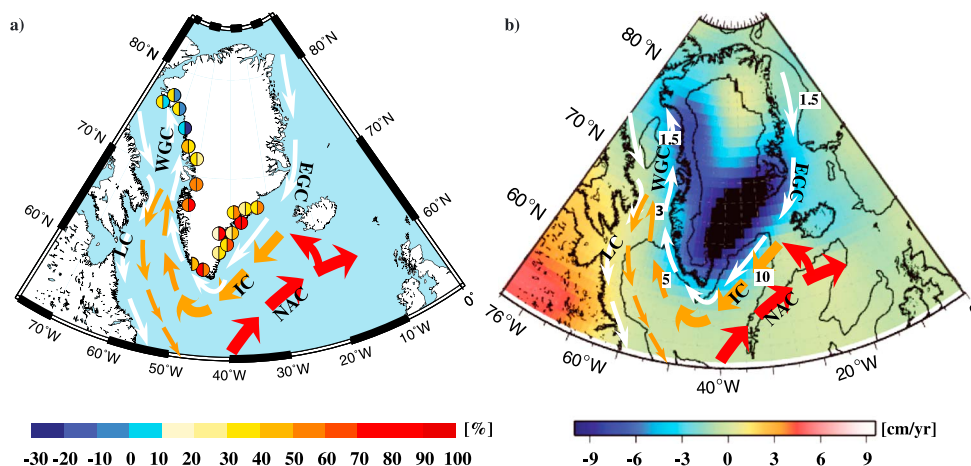
Figure 16. Relation between ocean currents, coastal uplift, and ice mass balance of coastal Greenland. Red arrows indicate the mean path of the warm North Atlantic Current (NAC); orange arrows indicate Irminger Current (IC), white arrows indicate East Greenland Current (EGC), West Greenland Current (WGC) and Labrador Current (LC). (a) Relative difference between uplift in 2010 and that in 2008 and 2009 as shown in Figure 15. Names of GPS stations were omitted here. (b) Mass loss in equivalent water height over Greenland between February 2003 and January 2008 observed by GRACE [*Wouters et al.*, 2008]. Numbers indicate the mean temperature (°C) of Atlantic-sourced waters on the Greenland shelf [*Straneo et al.*, 2012].

glaciers. This provides a useful tool for investigating the conditions of melting, and overall mass balance in Greenland, since most ice melting is concentrated in low elevation coastal ablation zones. The coastal "necklace" of high precision GPS stations emplaced and maintained by various geodetic institutions [*Bevis et al.*, 2012] thus provides an important tool for monitoring the health of the Greenland ice sheet.

[36] The role of warm sub-surface water in accelerating melting of marine-teminating glaciers was noted in Alaska [*Motyka et al.*, 2003] and Antarctica [*Payne et al.*, 2004; *Shepherd et al.*, 2004]. Warming ocean currents have been implicated in Greenland's accelerating mass loss since the late 1990s, through increased submarine melting, increased calving, and related dynamic effects [*Myers et al.*, 2007; *Holland et al.*, 2008; *Straneo et al.*, 2010, 2012; *Seale et al.*, 2011; *Joughin et al.*, 2012]. *Amundson et al.* [2010] pointed out that melting of the mélange in front of a calving glacier would reduce flow resistance for inland ice. *Motyka et al.* [2011] proposed that basal melting of a floating ice tongue would also increase calving and acceleration of inland ice. The warmest water found along the Greenland margin is fed by the IC, a branch of the North Atlantic Current, ultimately sourced from the Gulf Stream. The IC carries warm and saline subtropical water into subpolar basins and forms a key part of the subpolar gyre. As it approaches the Greenland coast, it meets cold, fresh polar melt water coast

that is lower in density, flowing south along the Greenland coast. At this point, the IC becomes a sub-surface current. The depth range of the IC is variable, but it typically occupies the depth range 100 m – 600 m (e.g., *Myers et al.*, 2007; *Holland et al.*, 2008; *Straneo et al.*, 2012). While cold, fresh polar water transported by the East and West Greenland Currents (EGC and WGC) is in direct contact with Greenland fjords (Figure 16), IW can nevertheless enter at the bottom of some glacier fjords, especially along the southeast and southwest coasts of Greenland, because it is more dense, reflecting its higher salinity.

[37] Our GPS data clearly illustrate the spatial distribution of IW influence: from mid-2007 to early 2011, on average, uplift acceleration is maximum for stations in southeast Greenland, where the IC first advects heat to coastal Greenland and then decreases as the current flows clockwise around Greenland (Figures 14c and 16a). Presumably, the influence of warm IW decreases to the northwest because it becomes diluted by mixing with cold coastal waters and exchange with cold atmosphere.

[38] There is a significant year-to-year variation in the amplitude of annual uplift in the southern coastal areas, with the variability decreasing to the north (Figures 5 and 12). The behavior of most sites in southeast and southwest Greenland closely follows the pattern of sub-surface ocean temperature variation between 2008 and 2010. In contrast, sites north of KAGA (69.2°N) do not experience significant

influence from warm IW during 2008 – 2010. Perhaps, the bathymetry of Davis Strait reduces IW influence north of that location. The bathymetry of Disco Bay, and the long, deep fjord of Jakobshavn Isbrae (near where KAGA is located) may also limit further northward penetration of warm water, by promoting mixing with cold surface waters. This is consistent with the oceanographic data of *Straneo et al.* [2012] showing only cold (< 3°C) intermediate water north of this location and consistent with the Hadley EN3 model output (Figure 8).

[39] Figure 16b shows mass loss in equivalent water height over Greenland between February 2003 and January 2008 observed by GRACE [*Wouters et al.*, 2008]. The location of maximum mass loss for this earlier period correlates with the point where the IC first turns towards Greenland, while mass loss decreases progressively northward along the west coast, implying that this is a long-lived (at least on the decadal time scale) pattern. The northern limit of IW influence on melting in northwest coastal Greenland will be an important variable for future monitoring.

[40] For the longer period of our observations, uplift and oceanic forcing are not well correlated (Figure 11c), suggesting nonlinearity between ice mass loss and oceanic forcing. One curious exception is KELY (Table 2 and Figure 11c). This site is located near a land-terminating glacier and exhibits good correlations between uplift and both CAPDD and AMSSWT, on both shorter (3 year) and longer (decadal) time scales (Figures 11 and 12). This station is located far from the coast (Figure 1 and Table 2), implying that mass loss should mainly be sensitive to atmospheric conditions. Its apparent correlation with offshore intermediate water temperature is puzzling.

[41] THU3, although located near marine-terminating glaciers, exhibits negative correlation with sub-surface water temperature (Figure 11). Also, small seasonal uplift variations are observed for other sites in northwest Greenland (KULL, DKSG, and MARG), and correlations between uplift and atmospheric or ocean temperature are not observed for these sites (Figure 12). Both air and water temperatures at these high latitudes are so low for most of the year that small fluctuations in these parameters may have little or no effect on summer melting. Perhaps longer-term ice dynamics plays an important role, e.g., ocean or atmosphere changes a decade ago or longer caused changes in the flow regime that are just now showing up. *Pritchard et al.* [2009] pointed out that unlike southeast Greenland, dynamic thinning in the northwest is caused by dynamic imbalance. This

dynamic imbalance may be associated with changes of ice thickness and surface slope [*Huybrechts and de Wolde*, 1999] caused by past climate forcing and may be a major influence on current mass loss and coastal uplift at these northwest sites, with warm summer conditions playing a secondary role.

[42] Using passive microwave data, *Box et al.* [2010] observed a longer duration melt season in 2010, with an earlier start (end of April) and later ending (mid September), compared to the 1997–2009 average value. Our data suggest longer melting season duration at some sites. However, the GPS uplift data also show anomalously fast uplift in 2010 (Figure 3d and Table 1), suggesting that ice melting proceeded not only by a lengthening of the melt season, but also by more intense summer melting. Anomalously warm atmospheric conditions in 2010 could be a contributing factor to intense summer melting, potentially increasing surface melt in the ablation zone [*Zwally et al.*, 2002]. Reduced albedo during the long melt season, with more days with exposed bare rock, may also have contributed to local mass loss [*Tedesco et al.*, 2011].

[43] *Murray et al.* [2010] showed that mass losses and speed of tidewater glaciers in southeast Greenland increased for 2003 – 2006 and then decreased for 2007–2008. Similarly, our GPS data show large uplift for 2003 – 2006 and small uplift for 2007 – 2008 at QAQ1 and KULU (Figure 3c). *Murray et al.* [2010] suggest that there is a negative feedback loop between calving and ocean temperature, as the icebergs eventually cool the water. This causes a ~2 year lag between initial speed up and mass loss (caused by influx of warm water) and subsequent slow down and decreased mass loss (caused by cooling of fjord and coastal water). Such "predator–prey" feedback relations are observed in many natural systems (e.g., *Walker et al.*, 1981; *Douglass and Knox*, 2005; *Koren and Feingold*, 2011). Future studies may be able to better examine such variations, since regional changes in short-term glacier response can now be studied in some detail using the techniques outlined here.

5. Conclusions

[44] We describe a new technique for investigating spatial and temporal variations of crustal uplift along coastal Greenland, allowing us to study annual variations in ice melting on a basin scale. Our data show large magnitude uplift for most GPS sites in 2010, indicating significant ice mass loss in that year, with the largest accelerations in southeast Greenland,

decreasing clockwise to the northwest, suggesting the influence of the warm IC. The pattern of relative uplift in 2008, 2009, and 2010 correlates with sub-surface ocean temperature until about 69°N (near KAGA), indicating that warm IW is sufficiently diluted with colder water north of this latitude that it has negligible influence on melting of marine-terminating outlet glaciers north of this point, during this time period. Ocean forcing is the dominant factor in coastal melting south of this point for both eastern and western Greenland. On the other hand, a few stations near land terminating glaciers also show large uplift, and by implication large mass losses in 2010. Thus, a combination of warm water and warm air contributed to the anomalously large ice mass loss in Greenland in 2010. Poor correlation between uplift and air temperature or ocean temperature at northwestern sites suggests that longer-term ice dynamics may be a significant controlling factor for ice mass change in northwestern Greenland.

Acknowledgments

References

Altamimi, Z., X. Collilieux, J. Legrand, B. Garayt, and C. Boucher (2007), ITRF2005: A new release of the International Terrestrial Reference Frame based on time series of station positions and Earth Orientation Parameters, *J. Geophys. Res.*, *112*, B09401, doi:10.1029/2007JB004949.

Amundson, J. M., M. Fahnestock, M. Truffer, J. Brown, M. P. Lüthi, and R. J. Motyka (2010), Ice mélange dynamics and implications for terminus stability, Jakobshavn Isbræ, Greenland, *J. Geophys. Res.*, *115*, F01005, doi:10.1029/2009JF001405.

Bennett, R. A. (2008), Instantaneous deformation from continuous GPS: Contributions from quasi-periodic loads, *Geophys. J. Int.*, *174*, 1052–1064, doi:10.1111/j.1365-246X.2008.03846.x.

Bevis, M. G., et al. (2012), Bedrock displacements in Greenland manifest ice mass variations, climate cycles and climate change, *Proc. Natl. Acad. Sci.*, *109*, 11944–11948, doi:10.1073/pnas.1204664109.

Blewitt, G. (2008), Fixed point theorems of GPS carrier phase ambiguity resolution and their application to massive network processing: Ambizap, *J. Geophys. Res.*, *113*, B12410, doi:10.1029/2008JB005736.

Boehm, J., A. Niell, P. Tregoning, and H. Schuh (2006), Global mapping function (GMF): A new empirical mapping function based on numerical weather model data, *Geophys. Res. Lett.*, *33*, L07304, doi:10.1029/2005GL025546.

Box, J. E., J. Cappelen, D. Decker, X. Fettweis, T. Mote, M. Tedesco, and R. S. W. van de Wal (2010), Greenland [in Arctic Report Card 2010], http://www.arctic.noaa.gov/reportcard.

Carstensen, L. S., and B. V. Jørgensen (2011), Weather and climate data from Greenland 1958–2010. DMI Technical Report 11-10. Ministry of Transport and Energy, Copenhagen, DK.

Chen, J. L., C. R. Wilson, and B. D. Tapley (2006), Satellite gravity measurements confirm accelerated melting of Greenland Ice Sheet, *Science*, *313*, 1958–1960, doi:10.1126/science.1129007.

Chen, J. L., C. R. Wilson, and B. D. Tapley (2011), Interannual variability of Greenland ice losses from satellite gravimetry, *J. Geophys. Res.*, *116*, B07406, doi:10.1029/2010JB007789.

Davis, J. L., B. P. Wernicke, S. Bisnath, N. A. Niemi, and P. Elósegui (2006), Subcontinental-scale crustal velocity changes along the Pacific-North American plate boundary, *Nature*, *441*(7097), 1131–1134, doi:10.1038/nature04781.

Davis, J. L., B. P. Wernicke, and M. E. Tamisiea (2012), On seasonal signals in geodetic time series, *J. Geophys. Res.*, *117*, B01403, doi:10.1029/2011JB008690.

Douglass, D. H., and R. S. Knox (2005). Climate forcing by the volcanic eruption of Mount Pinatubo. *Geophys. Res. Lett. 32*, L05710, doi:10.1029/02004GL022119.

Ettema, J., M. R. van den Broeke, E. van Meijgaard, W. J. van de Berg, J. L. Bamber, J. E. Box, and R. C. Bales (2009), Higher surface mass balance of the Greenland ice sheet revealed by high-resolution climate modeling, *Geophys. Res. Lett.*, *36*, L12501, doi:10.1029/2009GL038110.

Ettema, J., M. R. van den Broeke, E. van Meijgaard, and W. J. van de Berg (2010a), Climate of the Greenland ice sheet using a high-resolution climate model: Part 1. Evaluation, *Cryosphere*, *4*(2), 511–527, doi:10.5194/tc-4-511-2010.

Ettema, J. E., M. R. van den Broeke, E. van Meijgaard, W. J. van de Berg, J. E. Box, and K. Steffen (2010b), Climate of the Greenland ice sheet using a high-resolution climate model: Part 2. Near-surface climate and energy balance, *Cryosphere*, *4*, 529–544, doi:10.5194/tc-4-529-2010.

Hall, D. K., R. S. Williams Jr., S. B. Luthcke, and N. E. DiGirolamo (2008), Greenland ice sheet surface temperature, melt and mass loss: 2000–2006, *J. Glaciol.*, *54*, 81–93, doi:10.3189/002214308784409170.

Hanna, E., P. Huybrechts, I. Janssens, J. Cappelen, K. Steffen, and A. Stephens (2005), Runoff and mass balance of the Greenland ice sheet: 1958–2003, *J. Geophys. Res.*, *110*, D13108, doi:10.1029/2004JD005641.

Hanna, E., J. Cappelen, X. Fettweis, P. Huybrechts, A. Luckman, and M. H. Ribergaard (2009), Hydrologic response of the Greenland ice sheet: The role of oceanographic warming, *Hydrol. Process.*, *23*, 7–30, doi:10.1002/hyp.7090.

Holland, D. M., et al. (2008), Acceleration of Jakobshavn Isbræ triggered by warm subsurface ocean waters, *Nat. Geosci.*, *1*, 659–664, doi:10.1038/ngeo316.

Huybrechts, P., and J. de Wolde (1999). The dynamic response of the Greenland and Antarctic ice sheets to multiple-century climatic warming. *J. Climate*, *12*(8), 2169–2188.

Ingleby, B., and M. Huddleston (2007), Quality control of ocean temperature and salinity profiles – Historical and real-time data, *J. Marine Syst.*, *65*, 158–175.

Jacob, T., J. Wahr, W. T. Pfeffer, and S. Swenson (2012), Recent contributions of glaciers and ice caps to sea level rise, *Nature*, *482*(7386), 514–518, doi:10.1038/nature10847.

Jiang, Y., T. H. Dixon, and S. Wdowinski (2010), Accelerating uplift in the North Atlantic region as an indicator of ice loss, *Nat. Geosci.*, *3*, 404–407, doi:10.1038/ngeo845.

Joughin, I., R. B. Alley, and D. M. Holland. 2012. Ice-sheet response to oceanic forcing, *Science 338*, 1172–1176, doi:10.1126/science.1226481

Khan, S. A., J. Wahr, M. Bevis, I. Velicogna, and E. Kendrick (2010), Spread of ice mass loss into northwest Greenland observed by GRACE and GPS, *Geophys. Res. Lett.*, *37*, L06501, doi:10.1029/2010GL042460.

Koren, I., and G. Feingold (2011), Aerosol–cloud–precipitation system as a predator-prey problem, *Proc. Natl. Acad. Sci.*, *108*, 12,227–12,232, doi:10.1073/pnas.1101777108.

Krabill, W., et al. (2004), Greenland Ice Sheet: Increased coastal thinning, *Geophys. Res. Lett.*, *31*, L24402, doi:10.1029/2004GL021533.

Kuipers Munneke, P., M. R. van den Broeke, J. T. M. Lenaerts, M. G. Flanner, A. S. Gardner, and W. J. van de Berg (2011), A new albedo parameterization for use in climate models over the Antarctic ice sheet, *J. Geophys. Res.*, *116*, D05114, doi:10.1029/2010JD015113.

Letellier, T. (2004), Etude des ondes de marée sur les plateaux continentaux, Ph.D. thesis, Univ. de Toulouse III, Toulouse, France.

Luthcke, S. B., et al. (2006), Recent Greenland ice mass loss by drainage system from satellite gravity observations, *Science*, *314*, 1286–1289, doi:10.1126/science.1130776.

Motyka, R. J., L. Hunter, K. A. Echelmeyer, and C. Connor (2003), Submarine melting at the terminus of a temperate tidewater glacier, LeConte Glacier, Alaska, U.S.A, *Ann. Glaciol.*, *36*, 57–65, doi:10.3189/172756403781816374.

Motyka, R. J., M. Truffer, M. Fahnestock, J. Mortensen, S. Rysgaard, and I. Howat (2011), Submarine melting of the 1985 Jakobshavn Isbræ floating tongue and the triggering of the current retreat, *J. Geophys. Res.*, *116*, F01007, doi:10.1029/2009JF001632.

Murray, J. R., and P. Segall (2005), Spatiotemporal evolution of a transient slip event on the San Andreas fault near Parkfield, California, *J. Geophys. Res.*, *110*, B09407, doi:10.1029/2005JB003651.

Murray, T., et al. (2010), Ocean regulation hypothesis for glacier dynamics in southeast Greenland and implications for ice sheet mass changes, *J. Geophys. Res.*, *115*, F03026, doi:10.1029/2009JF001522.

Myers, P. G., N. Kulan, and M. H. Ribergaard (2007), Irminger Water variability in the West Greenland Current, *Geophys. Res. Lett.*, *34*, L17601, doi:10.1029/2007GL030419.

Payne, A. J., A. Vieli, A. P. Shepherd, D. J. Wingham, and E. Rignot (2004), Recent dramatic thinning of largest West Antarctic ice stream triggered by oceans, *Geophys. Res. Lett.*, *31*, L23401, doi:10.1029/2004GL021284.

Petrov, L., and J. P. Boy (2004), Study of the atmospheric pressure loading signal in very long baseline interferometry observations, *J. Geophys. Res.*, *109*, B03405, doi:10.1029/2003JB002500.

Pritchard, H. D., R. J. Arthern, D. G. Vaughan, and L. A. Edwards (2009), Extensive dynamic thinning on the margins of the Greenland and Antarctic ice sheets, *Nature*, *461*, 971–975.

Rignot, E., and Kanagaratnam, P. (2006), Changes in the velocity structure of the Greenland ice sheet, *Science*, *311*, 986–990, doi:10.1126/science.1121381.

Rignot, E., J. E. Box, E. Burgess, and E. Hanna (2008), Mass balance of the Greenland ice sheet from 1958 to 2007, *Geophys. Res. Lett.*, *35*, L20502, doi:10.1029/2008GL035417.

Schrama, E. J. O., and B. Wouters (2011), Revisiting Greenland ice sheet mass loss observed by GRACE, *J. Geophys. Res.*, *116*, B02407, doi:10.1029/2009JB006847.

Seale, A., P. Christoffersen, R. I. Mugford, and M. O'Leary (2011), Ocean forcing of the Greenland Ice Sheet: Calving fronts and patterns of retreat identified by automatic satellite monitoring of eastern outlet glaciers, *J. Geophys. Res.*, *116*, F03013, doi:10.1029/2010JF001847.

Shepherd, A., D. Wingham, and E. Rignot (2004), Warm ocean is eroding West Antarctic Ice Sheet, *Geophys. Res. Lett.*, *31*, L23402, doi:10.1029/2004GL021106.

Straneo, F., G. S. Hamilton, D. A. Sutherland, L. A. Stearns, F. Davidson, M. O. Hammill, G. B. Stenson, and A. Rosing-Asvid (2010), Rapid circulation of warm subtropical waters in a major glacial fjord in East Greenland. *Nat. Geosci.*, *3*(3), 182–186, doi:10.1038/ngeo764.

Straneo, F., D. Sutherland, D. Holland, C. Gladish, G. Hamilton, H. Johnson, E. Rignot, Y. Xu, M. Koppes (2012), Characteristics of ocean waters reaching Greenlands glaciers. *Ann. Glaciol.*, *53*(60), 202–210, doi:10.3189/2012AoG60A059.

Tedesco, M., X. Fettweis, M. R. van den Broeke, R. S. W. van de Wal, C. J. P. P. Smeets, W. J. van de Berg, M. C. Serreze, and J. E. Box. (2011), The role of albedo and accumulation in the 2010 melting record in Greenland, *Environ. Res. Lett.* *6*, 014005, doi:10.1088/1748-9326/6/1/014005

Thomas, R., E. Frederick, W. Krabill, S. Manizade, and C. Martin (2006), Progressive increase in ice loss from Greenland, *Geophys. Res. Lett.*, *33*, L10503, doi:10.1029/2006GL026075.

van Angelen, J. H., J. T. M. Lenaerts, S. Lhermitte, X. Fettweis, P. Kuipers Munneke, M. R. van den Broeke, E. van Meijgaard, and C. J. P. P. Smeets (2012), Sensitivity of Greenland Ice Sheet surface mass balance to surface albedo parameterization: a study with a regional climate model, *The Cryosphere*, *6*, 1175–1186, doi:10.5194/tc-6-1175-2012.

van de Wal, R. S. W., W. Boot, M. R. van den Broeke, C. J. P. P. Smeets, C. H. Reijmer, J. J. A. Donker, and J. Oerlemans (2008), Large and rapid melt-induced velocity changes in the ablation zone of the Greenland ice sheet, *Science*, *321*, 111–113, doi: 10.1126/science.1158540.

van den Broeke, M., J. Bamber, J. Ettema, E. Rignot, E. Schrama, W. J. van de Berg, E. van Meijgarrd, I. Velicogna, B. Wouters (2009), Partitioning recent Greenland mass loss, *Science*, *326*, 984–986, doi:10.1126/science.1178176.

Velicogna, I., and J. Wahr (2006), Acceleration of Greenland ice mass loss in spring 2004, *Nature*, *443*, 329–331, doi:10.1038/nature05168.

Velicogna, I. (2009), Increasing rates of ice mass loss from the Greenland and Antarctic ice sheets revealed by GRACE, *Geophys. Res. Lett.*, *36*, L19503, doi:10.1029/2009GL040222.

Walker, J. C. G., P. B., Hays, and J. F., Kasting (1981), A negative feedback mechanism for the long-term stabilization of Earth's surface temperature, *J. Geophys. Res. 86*, 9776–9782.

Wouters, B., D. Chambers, and E. J. O. Schrama (2008), GRACE observes small-scale mass loss in Greenland, *Geophys. Res. Lett.*, *35*, L20501, doi:10.1029/2008GL034816.

Zumberge, J. F., M. B. Heflin, D. C. Jefferson, M. M. Watkins, and F. H. Webb (1997), Precise point positioning for the efficient and robust analysis of GPS data from large networks, *J. Geophys. Res.*, *102*(B3), 5005–5017, doi:10.1029/96JB03860.

Zwally, H. J., W. Abdalati, T. Herring, K. Larson, J. Saba, and K. Steffen (2002), Surface melt-induced acceleration of Greenland ice sheet flow, *Science*, *297*(5579), 218–222, doi:10.1126/science.1072708.

Zwally, H. J., M. B. Giovinetto, J. Li, H. G. Cornejo, M. A. Beckley, A. C. Brenner, J. L. Saba, and D. H. Yi (2005), Mass changes of the Greenland and Antarctic ice sheets and shelves and contributions to sea-level rise: 1992–2002, *J. Glaciol.*, *51*, 509–527, doi:10.3189/172756505781829007.